Bright solitons in a spin-tensor-momentum-coupled Bose-Einstein condensate

Jie Sun,[1] Yuanyuan Chen,[1,*] Xi Chen,[1,2,†] and Yongping Zhang[1,‡]
[1]*International Center of Quantum Artificial Intelligence for Science and Technology (QuArtist) and Department of Physics, Shanghai University, Shanghai 200444, China*
[2]*Department of Physical Chemistry, University of the Basque Country UPV/EHU, Apartado 644, 48080 Bilbao, Spain*

(Received 23 January 2020; accepted 27 April 2020; published 13 May 2020)

Synthetic spin-tensor-momentum coupling has recently been proposed for realization in atomic Bose-Einstein condensates. Here we study bright solitons in Bose-Einstein condensates with spin-tensor-momentum coupling and spin-orbit coupling. The properties and dynamics of spin-tensor-momentum-coupled and spin-orbit-coupled bright solitons are identified to be different, which are contributed from the different symmetries.

DOI: 10.1103/PhysRevA.101.053621

I. INTRODUCTION

In ultracold neutral atoms, hyperfine spin states, coupling to linear momentum [1–7], or orbital angular momentum [8,9] are interesting and significant, not only in fundamental phenomena of ultracold atoms and condensed matter physics but also in the wide applications of quantum information processing [10], atom metrology [11], and atomtronics [12], with current experimental progress. In particularly, spin-orbit coupling (SOC) provides a unique dispersion relationship, exhibiting particular features without analogs in cases without SOC. The competition between repulsive nonlinearities stemming from atomic many-body interactions and the dispersion relation generates many fundamental ground-state phases, such as so-called stripe, plane-wave, and zero-momentum phases [13–20], and exotic collective excitations [21,22] in spin-orbit-coupled Bose-Einstein condensates (BECs).

Meanwhile, the interplay of nonlinearities and dispersions gives rise to the existence of solitons. Moreover, the SOC induces an inevitable modification of dispersion, resulting in different existence and properties of solitons. This motivates the active and exciting research prospect of the spin-orbit-coupled BEC solitons. The bright solitons are spatially localized, due to attractive nonlinearities, and have density profiles more or less reminiscent of ground states with repulsive nonlinearities [23,24]. In an analogous fashion, the one-dimensional spin-orbit-coupled plane-wave and striped solitons are formed under the action of combing SOC and Rabi coupling [25,26]. Their dynamics relevant to structural oscillations, shuttle motion, and transition between even and odd components are always accompanied by rich spin dynamics [27–29]. More importantly, the lack of Galilean invariance in spin-orbit-coupled systems [30] shows that it is nontrivial to find movable solitons; one cannot directly obtain a movable soliton from its stationary correspondence. The novel phenomenon is that SOC can stabilize two-dimensional bright solitons which always collapse due to self-attractions in ordinary BECs [31,32]. This provides an avenue to explore high-dimensional bright solitons in various physical scenarios [33–38]. High-dimensional defect states such as vortex, half-vortex, and skyrmion to spin-orbit-coupled cases have been further generalized as well in Refs. [39–44]. For instance, SOC can cast a force on vortex in compressible spin-orbit-coupled Bose-Einstein condensates [44]. In addition, there are several works devoted to spin-orbit-coupled spin-1/2, spin-1 [45–51], and spin-2 [52,53] BECs in various trap potentials, such as harmonic traps and periodic potentials [54–60]. In a slightly different but relevant respect, the dark solitons existing in spin-orbit-coupled BECs are also interesting for exploring their dynamics [49,61,62].

Very recently, the generation of artificial spin-tensor-momentum coupling (STMC) into an atomic BEC has been proposed [63]. Different from the usual spin-orbit coupling where linear momentum is coupled with spin vectors, STMC is the interaction between linear momentum and spin tensors. This emergent interaction can be applicable to the discovery of dynamical stripe states, STMC fermionic superfluids, and exotic topological matters [64,65]. The motivation of this paper is to investigate the bright solitons in spin-tensor-momentum-coupled BECs, where the three components of ground hyperfine states for ^{87}Rb atoms are utilized for experimental implementation. We first apply the imaginary-time evolution method and variational method to study stationary properties of spin-tensor-momentum-coupled solitons and further explore their dynamics triggered by two different approaches. By comparing with density profiles and dynamics of spin-tensor-momentum-coupled and spin-orbit-coupled bright solitons, we conclude that the difference between them originates from the different symmetry relevant to spin rotation.

The paper will be organized as follows. In Sec. II the systems and Hamiltonian are introduced for both SOC and STMC for completeness and further comparison. Later, the bright solitons are discussed for both spin-tensor-momentum-coupled and spin-orbit-coupled BECs in Sec. III to clarify the difference in the spin rotation and symmetry. Finally, the conclusion is briefly made in Sec. IV.

*cyyuan@staff.shu.edu.cn
†xchen@shu.edu.cn
‡yongping11@t.shu.edu.cn

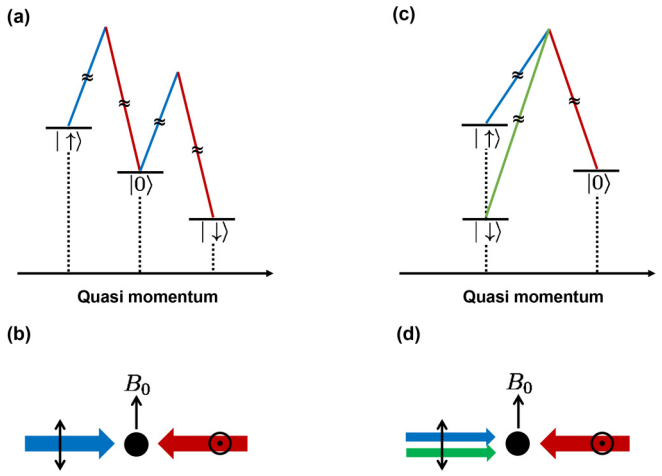

FIG. 1. Experimental schemes to realize the spin-orbit coupling (a), (b) and spin-tensor-momentum coupling (c), (d). Three hyperfine states ($|\uparrow\rangle, |0\rangle, |\downarrow\rangle$) are split by a bias magnetic field B_0. In (a), (b) two laser beams propagate oppositely to couple $|p_x - 2\hbar k_{\rm R}, \uparrow\rangle$, $|p_x, 0\rangle, |p_x + 2\hbar k_{\rm R}, \downarrow\rangle$, with p_x being momentum along the laser direction and quasimomentum $2\hbar k_{\rm R}$ relevant to the wave number of lasers, where the quasimomentum difference between hyperfine states constitutes the spin-orbit coupling. In (c), (d) two beams whose polarizations are parallel to the bias magnetic field propagate along the same direction and the third beam in the opposite direction. They can couple $|p_x - 2\hbar k_{\rm R}, \uparrow\rangle, |p_x, 0\rangle, |p_x - 2\hbar k_{\rm R}, \downarrow\rangle$.

II. MODEL AND HAMILTONIAN

We first consider the experiment of synthetic SOC in three-component BECs [66,67] where the three hyperfine states of ^{87}Rb atoms are utilized with the energy splitting by a bias magnetic field, as shown in Figs. 1(a) and 1(b). To realize SOC, the atoms are dressed by two counterpropagating Raman laser beams and the polarizations of lasers are arranged so that two-photon optical transitions can be induced; see Fig. 1(b). The transitions in the basis of ($|\uparrow\rangle = |1,-1\rangle, |0\rangle = |1,0\rangle, |\downarrow\rangle = |1,1\rangle$) are engineered as

$$H_{\rm Ram}^{\rm SOC} = \Omega \begin{pmatrix} 0 & e^{-i2k_{\rm R}x} & 0 \\ e^{i2k_{\rm R}x} & 0 & e^{-i2k_{\rm R}x} \\ 0 & e^{i2k_{\rm R}x} & 0 \end{pmatrix},$$

where Ω is the strength of two-photon Rabi coupling [68]. During the transitions, there is a momentum $2\hbar k_{\rm R}$ exchange between the atoms and lasers, here $k_{\rm R} = 2\pi/\lambda_{\rm R}$ with $\lambda_{\rm R}$ being the wavelength of Raman lasers. Including kinetic energy, the Hamiltonian becomes, $H_{\rm SOC} = p_x^2/2m + H_{\rm Ram}^{\rm SOC}$, with m being atomic mass and p_x being momentum along the direction of Raman lasers. To explicitly show the existence of SOC, a unitary transformation is needed, $U_{\rm SOC} = e^{i2k_{\rm R}xF_z}$, such that the Hamiltonian $\tilde{H}_{\rm SOC} = U_{\rm SOC} H_{\rm SOC} U_{\rm SOC}^{-1}$ becomes

$$\tilde{H}_{\rm SOC} = \frac{p_x^2}{2m} - \frac{4\hbar k_{\rm R} p_x F_z}{2m} + \frac{4(\hbar k_{\rm R})^2 F_z^2}{2m} + \sqrt{2}\Omega F_x. \quad (1)$$

Here (F_x, F_y, F_z) are spin-1 Pauli matrices, and the SOC $2\hbar k_{\rm R} p_x F_z/m$ is involved. Physically, the SOC means that there is a quasimomentum difference $-2\hbar k_{\rm R}$ between states $|\uparrow\rangle$ and $|0\rangle$, and between $|0\rangle$ and $|\downarrow\rangle$.

Next, the STMC can be introduced artificially by dressing the atoms with three Raman beams [63], see Figs. 1(c) and 1(d). Two of them with the same linear polarization propagate along the same direction, and the other propagates oppositely. The two-photon transitions accompanying momentum transfers become

$$H_{\rm Ram}^{\rm STMC} = \Omega \begin{pmatrix} 0 & e^{-i2k_{\rm R}x} & 0 \\ e^{i2k_{\rm R}x} & 0 & e^{i2k_{\rm R}x} \\ 0 & e^{-i2k_{\rm R}x} & 0 \end{pmatrix}.$$

Note that the difference between $H_{\rm Ram}^{\rm SOC}$ and $H_{\rm Ram}^{\rm STMC}$ is very slight. To eliminate the spatial dependence in $H_{\rm Ram}^{\rm STMC}$, a unitary transformation $U_{\rm STMC} = e^{i2k_{\rm R}xF_z^2}$ is performed, and the new total Hamiltonian $\tilde{H}_{\rm STMC} = U_{\rm STMC} H_{\rm STMC} U_{\rm STMC}^{-1}$ with $H_{\rm STMC} = p_x^2/2m + H_{\rm Ram}^{\rm STMC}$ is expressed as

$$\tilde{H}_{\rm STMC} = \frac{p_x^2}{2m} - \frac{4\hbar k_{\rm R} p_x F_z^2}{2m} + \frac{4(\hbar k_{\rm R})^2 F_z^2}{2m} + \sqrt{2}\Omega F_x. \quad (2)$$

The STMC takes a specific form as $2\hbar k_{\rm R} p_x F_z^2/m$. From the above equation, it is clear that such specific STMC is just a rearrangement of the quasimomentum difference comparing with the case of the SOC. The quasimomentum difference between $|\uparrow\rangle$ and $|0\rangle$ is $-2\hbar k_{\rm R}$, while it is $2\hbar k_{\rm R}$ between $|0\rangle$ and $|\downarrow\rangle$.

III. BRIGHT SOLITONS WITH STMC AND SOC

Now, we are ready to study bright solitons in the BECs with both STMC and SOC whose experimental realizations are analyzed in the previous section, Sec. II. We start from the standard Gross-Pitaevskii (GP) equations and take into consideration the spin-tensor-momentum-coupled and spin-orbit-coupled Hamiltonian in Eqs. (1) and (2). The dimensionless GP equations for spin-tensor-momentum-coupled BEC are

$$i\frac{\partial \Psi}{\partial t} = \left[-\partial_x^2 + (4i\partial_x + 4 + \Delta)F_z^2 + \sqrt{2}\Omega F_x + H_{\rm int}\right]\Psi, \quad (3)$$

while the spin-orbit-coupled GP equations are

$$i\frac{\partial \Psi}{\partial t} = \left[-\partial_x^2 + 4i\partial_x F_z + (4 + \Delta)F_z^2 + \sqrt{2}\Omega F_x + H_{\rm int}\right]\Psi. \quad (4)$$

In both equations, the units of energy, position coordinate, and time that we adopt are $\hbar^2 k_{\rm R}^2/2m$, $1/k_{\rm R}$ and $2m/\hbar k_{\rm R}^2$, respectively. The additional term ΔF_z^2 originates from the quadratic Zeeman effect. Three-component wave functions are $\Psi = (\Psi_\uparrow, \Psi_0, \Psi_\downarrow)^T$, for convenience; in the following, we relabel the wave functions as $\Psi = (\Psi_1, \Psi_2, \Psi_3)^T$. In the above equations, $H_{\rm int} = g_0(|\Psi_1|^2 + |\Psi_2|^2 + |\Psi_3|^2)$, for simplicity, and we consider that inter- and intraspecies interaction coefficients are the same and equal to g_0. Since our aim is to investigate bright solitons, we focus on the attractive interactions of $g_0 < 0$. In experiments, attractive interactions can be realized by standard Feshbach resonance technique.

The difference between the spin-tensor-momentum-coupled and spin-orbit-coupled GP equations is the appearance of $4i\partial_x F_z^2$ and $4i\partial_x F_z$. Such a difference leads to different symmetries of GP equations, which affects the properties of bright solitons. Since the systems are

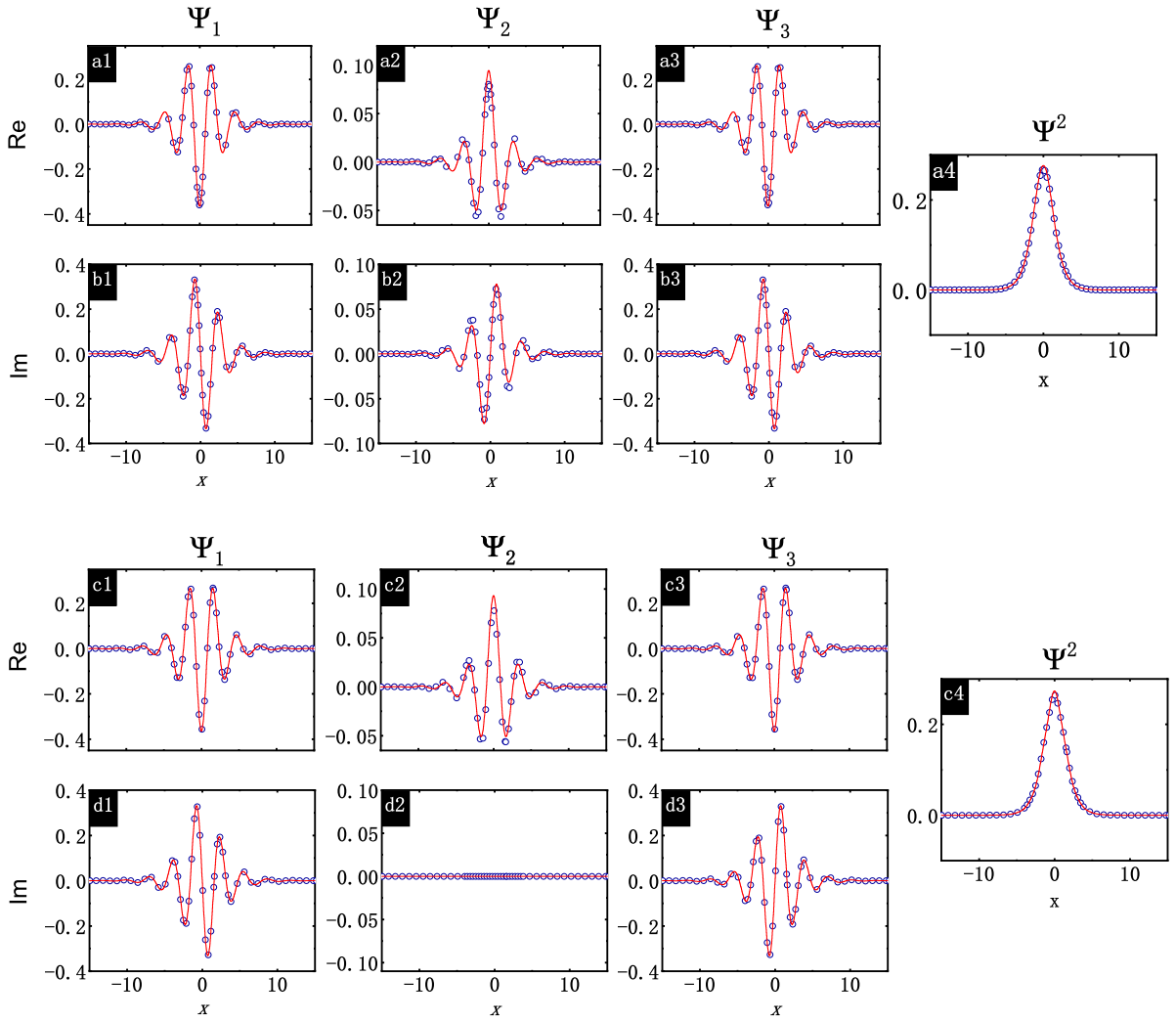

FIG. 2. Profiles of the spin-tensor-momentum-coupled (upper panel) and spin-orbit-coupled (lower panel) bright solitons. In each panel, the first (second) row is the real (imaginary) parts of soliton wave functions $\Psi = (\Psi_1, \Psi_2, \Psi_3)^T$. (a4, c4) The total density distributions $|\Psi_1|^2 + |\Psi_2|^2 + |\Psi_3|^2$. Solid lines are solutions from the imaginary-time evolution method, and circles are analytical solutions from the variational method. The dimensionless parameters are $\Delta = -1$, $\Omega = 0.5$ and $g_0 = -2$.

one dimensional with attractive nonlinearities, ground states are bright solitons. We find stationary bright solitons by the numerical calculation of GP equations using the imaginary-time evolution method, which is a standard routine to get ground states. Typical soliton profiles are demonstrated in Fig. 2. The upper panel shows the profiles of spin-tensor-momentum-coupled solitons, and the lower panel is that of spin-orbit-coupled solitons. For further comparison, we adopt the same parameters for the GP equations with STMC and SOC. Our general observation is that the imaginary parts of soliton wave functions for both STMC and SOC do not vanish. In contrast, the ground states of ordinary BECs (without STMC or SOC) are real-valued with no node in wave functions [15]. This is the unique feature of spin-orbit-coupled [24] and spin-tensor-momentum-coupled BECs. At first sight, the spin-tensor-momentum-coupled solitons share the same profiles with spin-orbit-coupled solitons, specifically, the real parts of soliton wave functions are almost the same. However, there exists an apparent difference in the imaginary parts.

We find that bright solitons follow symmetries of the systems. The stationary spin-tensor-momentum-coupled GP equations in Eq. (3) have a spin-rotating symmetry,

$$\mathcal{R}_{\mathrm{STMC}} = e^{i\pi F_x} = \begin{pmatrix} 0 & 0 & -1 \\ 0 & -1 & 0 \\ -1 & 0 & 0 \end{pmatrix}, \tag{5}$$

which rotates spins along the F_x axis by the angle of π, and a joint parity symmetry,

$$\mathcal{O}_{\mathrm{STMC}} = \mathcal{P}\mathcal{K}, \tag{6}$$

with $\mathcal{P}$ and $\mathcal{K}$ being the parity and complex conjugate operators. The symmetry $\mathcal{R}_{\mathrm{STMC}}$ is relevant to the spin tensor F_x^2, since $F_x^2 = \frac{1}{2}(\mathbb{I} - \mathcal{R}_{\mathrm{STMC}})$. The eigenequation is $\mathcal{R}_{\mathrm{STMC}}\Psi = \pm\Psi$. For the $+1$ eigenstate, $\Psi_2(x) = 0$, which leads to $\langle F_x \rangle = 0$, whereas to minimize the energy of the Rabi coupling term $\sqrt{2}\Omega F_x$, it is preferable that $\langle F_x \rangle < 0$. Therefore, bright solitons select the eigenstate with -1 eigenvalue, $\mathcal{R}_{\mathrm{STMC}}\Psi = -\Psi$, the consequence of which is $\Psi_1(x) = \Psi_3(x)$. Figure 2

demonstrates $\Psi_1(x) = \Psi_3(x)$ from the real and imaginary parts. The symmetry $\mathcal{O}_{\rm STMC}$ determines that the parity of real parts of soliton wave functions Ψ_1, Ψ_2, and Ψ_3 should be opposite to that of the imaginary parts. The real parts are even and imaginary parts are odd; see Fig. 2.

The symmetry of the stationary spin-orbit-coupled GP equations in Eq. (4) is slightly different from the case of the STMC. The spin-orbit-coupled equations possess a particular spin-rotating symmetry,

$$\mathcal{R}_{\rm SOC} = \mathcal{P}e^{i\pi F_x} = \mathcal{P}\begin{pmatrix} 0 & 0 & -1 \\ 0 & -1 & 0 \\ -1 & 0 & 0 \end{pmatrix}, \tag{7}$$

which must be the joint of spin rotation and parity. The equations also have the symmetry $\mathcal{PK}$, which is the same as the spin-tensor-momentum-coupled case, so the parity of real and imaginary parts of spin-orbit-coupled solitons are even and odd, respectively, which can be confirmed from Fig. 2. For the eigenequation of $\mathcal{R}_{\rm SOC}$ is $\mathcal{R}_{\rm SOC}\Psi(x) = \pm\Psi(x)$, taking into account the parity of real and imaginary parts of wave functions, solitons choose the eigenstate with -1 eigenvalue; if they choose the state with $+1$ eigenvalue, then $\langle F_x\rangle = 0$ and the Rabi coupling energy cannot be minimized. With -1 eigenvalue, the symmetry $\mathcal{R}_{\rm SOC}$ requires that $\Psi_1(x) = \Psi_3(-x)$ and $\Psi_2(x) = \Psi_2(-x)$. Finally, because of the parity from $\mathcal{PK}$, the real parts of $\Psi_1(x)$ and $\Psi_3(x)$ become equal and the imaginary parts of $\Psi_1(x)$ and $\Psi_3(x)$ have opposite signs, while the imaginary part of $\Psi_2(x)$ must disappear.

The above symmetry analysis provides a deep insight into the understanding of solitons. So, we are motivated to apply a variational function to stimulate corresponding solitons as follows. For the spin-tensor-momentum-coupled soliton, the variational wave function is

$$\Psi_{\rm STMC} = \begin{pmatrix} A[\cos(k_1x) + i\rho_0\sin(k_1x)] \\ B[\cos(k_2x) + i\rho_1\sin(k_2x)] \\ A[\cos(k_1x) + i\rho_0\sin(k_1x)] \end{pmatrix}\mathrm{sech}(\sigma x). \tag{8}$$

This trial wave function completely satisfies the symmetries of $\mathcal{R}_{\rm STMC}$ and $\mathcal{O}_{\rm STMC}$. Variational parameters A, B, k_1, k_2, ρ_0, ρ_1, and σ would be determined by the minimization of the total energy $E_{\rm STMC} = \int dx(E_0 + \bar{E}_{\rm STMC})$, with the energy density

$$\begin{aligned} E_0 =& |\partial_x\Psi_1|^2 + |\partial_x\Psi_2|^2 + |\partial_x\Psi_3|^2 + (\Delta+4)(|\Psi_1|^2 \\ &+ |\Psi_3|^2) + \Omega\left(\Psi_1\Psi_2^* + \Psi_1^*\Psi_2 + \Psi_2\Psi_3^* + \Psi_2^*\Psi_3\right) \\ &+ \frac{g_0}{2}(|\Psi_1|^2 + |\Psi_2|^2 + |\Psi_3|^2)^2, \end{aligned} \tag{9}$$

and

$$\bar{E}_{\rm STMC} = 4i(\Psi_1^*\partial_x\Psi_1 + \Psi_3^*\partial_x\Psi_3). \tag{10}$$

Considering the symmetries of $\mathcal{R}_{\rm SOC}$ and $\mathcal{PK}$, the variational wave function for a spin-orbit-coupled soliton might be

$$\Psi_{\rm SOC} = \begin{pmatrix} A[\cos(k_1x) + i\rho_0\sin(k_1x)] \\ B\cos(k_2x) \\ A[\cos(k_1x) - i\rho_0\sin(k_1x)] \end{pmatrix}\mathrm{sech}(\sigma x). \tag{11}$$

All unknown quantities appearing in above function should be determined by the minimization of the energy $E_{\rm SOC} = \int dx(E_0 + \bar{E}_{\rm SOC})$, where the spin-orbit-coupled energy density is

$$\bar{E}_{\rm SOC} = 4i(\Psi_1^*\partial_x\Psi_1 - \Psi_3^*\partial_x\Psi_3). \tag{12}$$

The results from a variational approximation approach for both spin-tensor-momentum-coupled and spin-orbit-coupled solitons are shown by circles in Fig. 2. Obviously, the variational wave functions are consistent with the results from the imaginary-time evolution method, as discussed before. We also checked other parameters, and the results from these two methods match well.

We characterize the properties of bright solitons by the variational wave functions. The features are identified by the dependence of k_1, k_2, σ and the total energy $E_{\rm STMC}$ and $E_{\rm SOC}$ on the variables of Δ and Ω. Here we choose Δ and Ω as free parameters, since they can be tuned in experiments easily; Δ can be modified by changing the bias magnetic field and Ω can be changed by adjusting the Raman laser intensity. The results are described in Fig. 3. The magnitudes of k_1 and k_2 are relevant to the number of nodes in soliton profiles. The larger k_1 and k_2 induce more oscillations in the real and imaginary parts of the soliton wave functions, see Fig. 2. This type of oscillation reveals the exotic properties of STMC ($4i\partial_xF_z^2$) and SOC ($4i\partial_xF_z$). Because of the competition between $4i\partial_xF_z^2$ ($4i\partial_xF_z$) and $(\Delta+4)F_z^2$ or $\sqrt{2}\Omega F_x$, large Δ and Ω suppress the effect of the STMC and SOC, thus reducing the oscillation nodes. As a result, k_1 or k_2 decrease with increasing Δ or Ω. This somehow explains the tendency of lines in Figs. 3(a1)–3(d2). In addition, the modification of k_1 and k_2, and the Rabi coupling $\sqrt{2}\Omega F_x$ also make soliton wave packets more spatially localized to reduce oscillations. Finally, as shown in Figs. 3(b3) and 3(d3), σ increases with increasing Ω. However, the dependence of σ on Δ is not monotonous at all, see Figs. 3(a3) and 3(c3), resulting in two obvious slopes in the total energy as a function of Δ in Figs. 3(a4) and 3(c4). Figures 3(b4) and 3(d4) demonstrate that Ω always reduces the total energy because the Rabi coupling energy is proportional to $\langle F_x\rangle$, satisfying $\langle F_x\rangle < 0$. In the last column of Fig. 3, we also demonstrate that the results calculated from the imaginary-time evolution method (red circles) are consistent with those from variational approximation (blue solid line).

In the following, we turn to the dynamics of spin-tensor-momentum-coupled and spin-orbit-coupled solitons, after we show the stationary properties of bright solitons and find that solitons have well-defined symmetries. Two kinds of dynamics, triggered by different approaches, are numerically studied by solving the time evolution of Eq. (3) or (4) with stationary solitons as initial states. First of all, we study quench dynamics by suddenly switching off the STMC or SOC. The results are shown in Fig. 4. Figures 4(a) and 4(b) correspond to the spin-tensor-momentum-coupled and the spin-orbit-coupled solitons, respectively. After switching off the STMC or SOC, solitons are not stationary. This provides clear evidence that the solitons are intrinsically supported by the STMC or SOC. Interestingly, the time evolution of the spin-tensor-momentum-coupled and spin-orbit-coupled solitons are that different. The spin-tensor-momentum-coupled soliton moves along one direction, while the spin-orbit-coupled soliton splits into two parts with opposite velocities. This is because that

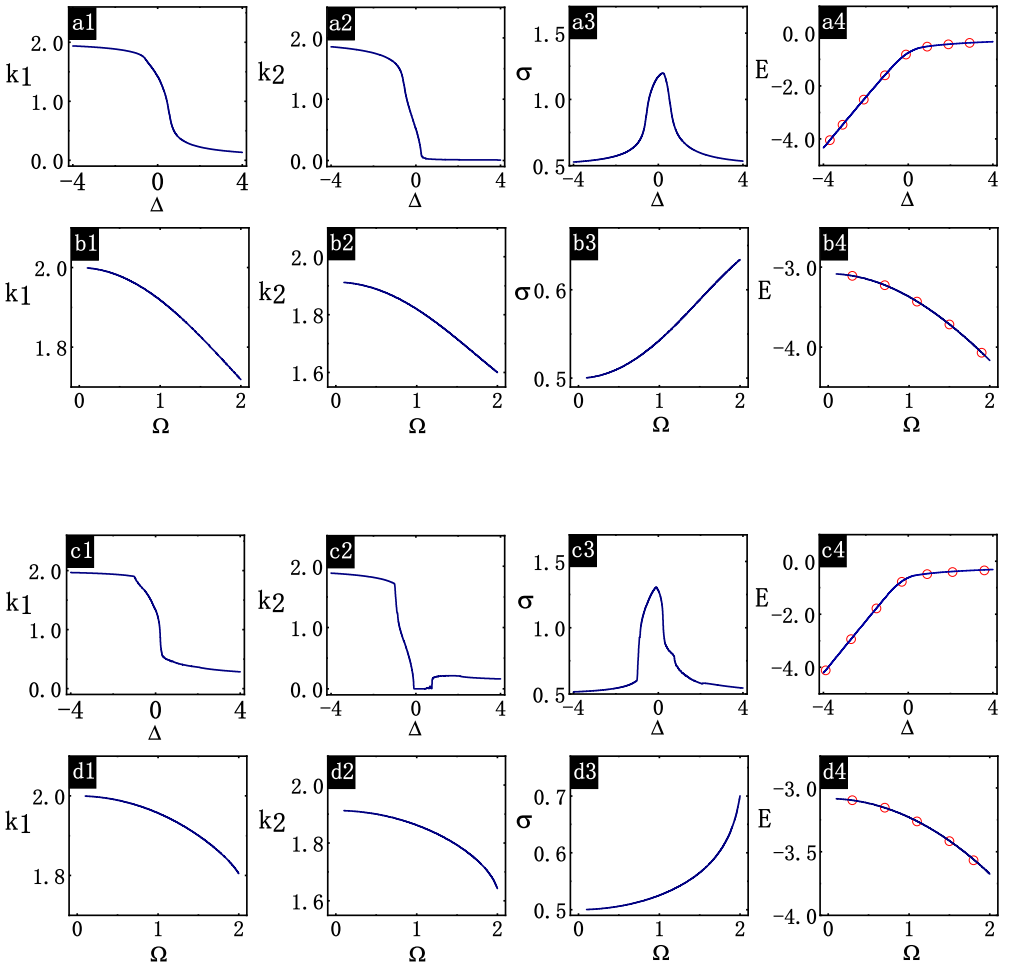

FIG. 3. Features of the spin-tensor-momentum-coupled (upper panel) and spin-orbit-coupled (lower panel) bright solitons characterized from variational wave functions. The variational parameters k_1, k_2, σ and total energy $E_{\mathrm{STMC}}, E_{\mathrm{SOC}}$ are a function of Δ and Ω. Solid lines are from the variational method, and circles are from the imaginary-time evolution method. In the first (second) row of each panel, $\Omega = 1$ ($\Delta = -3$). The nonlinear coefficient is $g_0 = -2$. In the last column, we also demonstrate that the results calculated from imaginary-time evolution method (red circles) and variational approximation (blue solid line) match quite well.

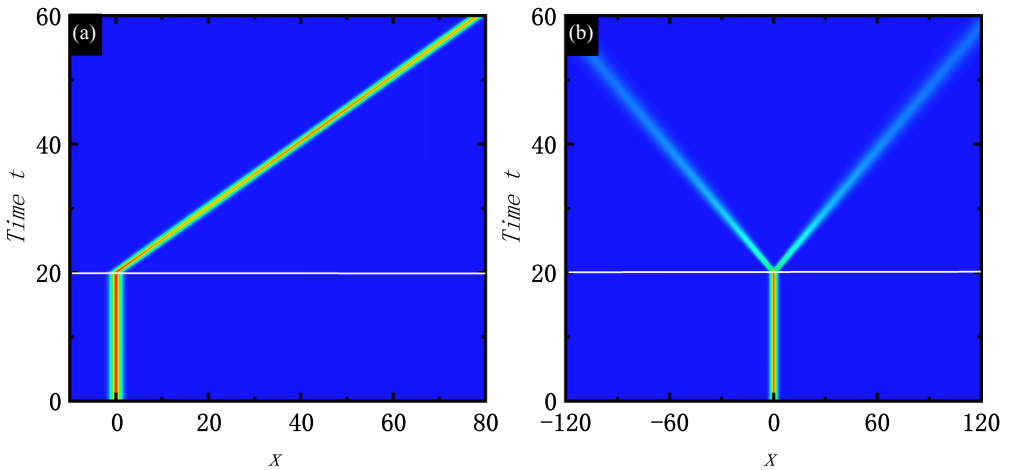

FIG. 4. The time evolution of initially prepared spin-tensor-momentum-coupled (a) and spin-orbit-coupled (b) solitons. The horizontal lines at $t = 20$ are a guide for the eye, at which STMC and SOC are suddenly switched off, respectively. The total density $|\Psi|^2 = |\Psi_1|^2 + |\Psi_2|^2 + |\Psi_3|^2$ is demonstrated. The parameters are $\Delta = -1$, $\Omega = 0.5$ and $g_0 = -2$.

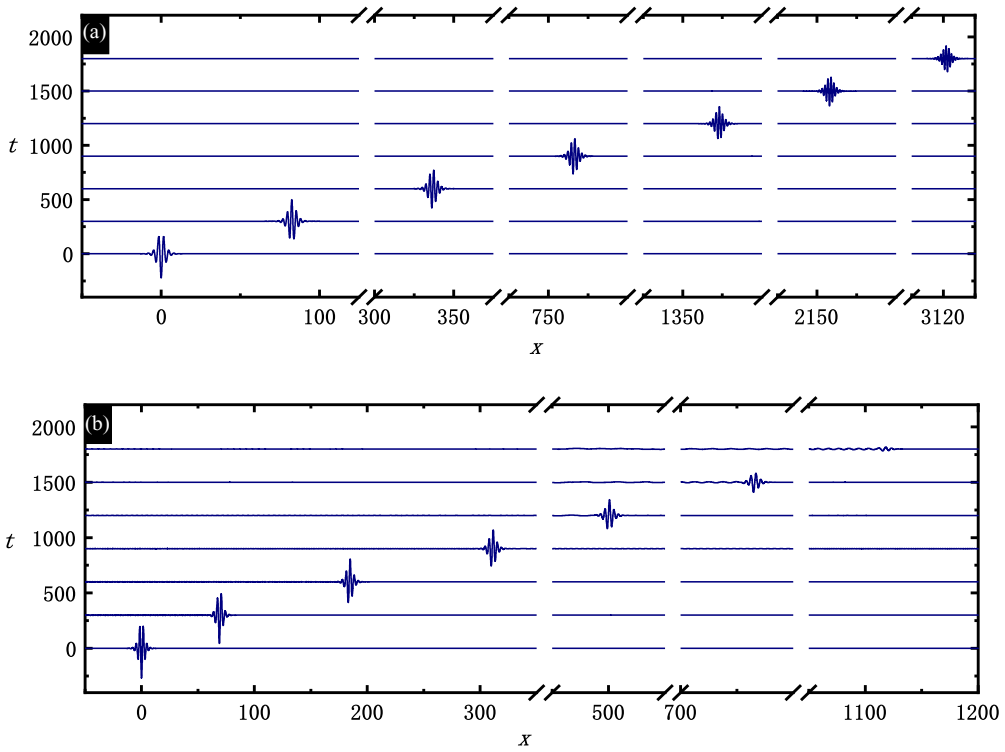

FIG. 5. The time evolution of spin-tensor-momentum-coupled (a) and spin-orbit-coupled (b) solitons initiated by a constant weak acceleration force which is implemented by adding a linear potential $-0.001x$ into GP equations in Eqs. (3) and (4). The parameters are $\Delta = -1$, $\Omega = 0.5$ and $g_0 = -2$. The profile of the real part of Ψ_1 is shown. All data are plotted as two dimensional, but the amplitude of real part is not labeled here for simplicity.

the initial soliton satisfies $k_1 = k_2$, $\rho_0 = \rho_1 = 1$. Therefore, the spin-tensor-momentum-coupled soliton is the spatial confinement of a plane wave; after tuning off the STMC, it moves in the direction of the plane wave, while the spin-orbit-coupled soliton includes two plane-wave modes due to the component $\Psi_2 \propto \cos(k_2 x) = (e^{ik_2 x} + e^{-ik_2 x})/2$. The Rabi coupling transfers these two plane-wave modes into other components, leading to the splitting of two branches during the evolution.

Secondly, we shall explore the acceleration of bright solitons. We add a constant weak force to accelerate the initially prepared solitons. In experiments, such constant force can be implemented by gravity. For the numerical stimulation, we add a new term Fx in the Hamiltonians (1) and (2), with F being the constant force. The slow adiabatic acceleration connects moving bright solitons to stationary bright solitons [24]. Due to the lack of Galilean invariance in spin-tensor-momentum-coupled and spin-orbit-coupled systems, the profiles of moving solitons becomes different from those of stationary solitons; therefore they are changed during the acceleration, as illustrated in Fig. 5. The change of the spin-orbit-coupled soliton is more pronounced than that of the spin-tensor-momentum-coupled soliton, also see Fig. 5. We provide a simple insight into the understanding of such a difference. The solution of a moving bright soliton should be

$$\Psi(x,t) = \Phi_v(x - 2vt, t)e^{ivx - iv^2 t}, \tag{13}$$

with v being the moving velocity. Substituting this ansatz into GP equations in Eqs. (3) and (4), the resulting equations for $\Phi_v(x - 2vt, t)$ are different from the original ones by the additional appearance of $-4vF_z^2$ and $-4vF_z$, respectively, for the spin-tensor-momentum-coupled and spin-orbit-coupled equations. The additional $-4vF_z^2$ does not have an effect on the symmetry $\mathcal{R}_{\mathrm{STMC}}$, so the moving spin-tensor-momentum-coupled bright solitons still possess $\mathcal{R}_{\mathrm{STMC}}$. In contrast, $-4vF_z$ for the spin-orbit-coupled solitons breaks the symmetry $\mathcal{R}_{\mathrm{SOC}}$. The constant acceleration force linearly increases the velocities of solitons. However, the symmetry $\mathcal{R}_{\mathrm{STMC}}$ manages to protect the profiles of the bright soliton, thus avoiding dramatic change. The initial stationary spin-orbit-coupled bright soliton changes distinctly during the acceleration, since the symmetry of the stationary one is so different from that of the moving one.

IV. CONCLUSION

We systematically study bright solitons in three-component BECs with the spin-tensor-momentum coupling and spin-orbit coupling, motivated by the rapid development of the research field of spin-orbit-coupled ultracold atomic gases and by the recent proposal to realize the spin-tensor-momentum-coupled BEC. The slight difference between the STMC and SOC leads to various symmetries which give rise to different profiles of soliton wave functions. Moreover, the dynamics of spin-tensor-momentum-coupled and spin-orbit-coupled solitons are different during the time evolution when they are initiated by switching off the couplings or by a constant weak acceleration force. We conclude that all different properties come from different symmetries.

ACKNOWLEDGMENTS

We sincerely acknowledge Yong Xu, Biao Wu, and Ray-Kuang Lee for helpful discussions. This work was supported by the NSFC (Grants No. 11974235, No. 1174219, and No. 11474193), the Thousand Young Talents Program of China, SMSTC (Grants No. 2019SHZDZX01-ZX04, No. 18010500400, and No. 18ZR1415500), and the Program for Professor of Special Appointment (Eastern Scholar) at Shanghai Institutions of Higher Learning and Shuguang Program (Program No. 17SG39). X.C. is also grateful for support from the Ramón y Cajal program of the Spanish MINECO (RYC-2017-22482).

[1] Y.-J. Lin, K. Jiménez-García, and I. B. Spielman, Spin-orbit-coupled Bose-Einstein condensates, Nature (London) **471**, 83 (2011).

[2] J.-Y. Zhang, S.-C. Ji, Z. Chen, L. Zhang, Z.-D. Du, B. Yan, G.-S. Pan, B. Zhao, Y.-J. Deng, H. Zhai, S. Chen, and J.-W. Pan, Collective Dipole Oscillations of a Spin-Orbit Coupled Bose-Einstein Condensate, Phys. Rev. Lett. **109**, 115301 (2012).

[3] P. Wang, Z.-Q. Yu, Z. Fu, J. Miao, L. Huang, S. Chai, H. Zhai, and J. Zhang, Spin-Orbit Coupled Degenerate Fermi Gases, Phys. Rev. Lett. **109**, 095301 (2012).

[4] L. W. Cheuk, A. T. Sommer, Z. Hadzibabic, T. Yefsah, W. S. Bakr, and M. W. Zwierlein, Spin-Injection Spectroscopy of a Spin-Orbit Coupled Fermi Gas, Phys. Rev. Lett. **109**, 095302 (2012).

[5] C. Qu, C. Hamner, M. Gong, C. Zhang, and P. Engels, Observation of *Zitterbewegung* in a spin-orbit-coupled Bose-Einstein condensate, Phys. Rev. A **88**, 021604(R) (2013).

[6] A. J. Olson, S.-J. Wang, R. J. Niffenegger, C.-H. Li, C. H. Greene, and Y. P. Chen, Tunable Landau-Zener transitions in a spin-orbit-coupled Bose-Einstein condensate, Phys. Rev. A **90**, 013616 (2014).

[7] C. Hamner, C. Qu, Y. Zhang, J. J. Chang, M. Gong, C. Zhang, and P. Engels, Dicke-type phase transition in a spin-orbit-coupled Bose-Einstein condensate, Nat. Commun. **5**, 4023 (2014).

[8] H.-R. Chen, K.-Y. Lin, P.-K. Chen, N.-C. Chiu, J.-B. Wang, C.-A. Chen, P.-P. Huang, S.-K. Yip, Y. Kawaguchi, and Y.-J. Lin, Spin-Orbital-Angular-Momentum Coupled Bose-Einstein Condensates, Phys. Rev. Lett. **121**, 113204 (2018).

[9] D. Zhang, T. Gao, P. Zou, L. Kong, R. Li, X. Shen, X.-L. Chen, S.-G. Peng, M. Zhan, H. Pu, and K. Jiang, Ground-State Phase Diagram of a Spin-Orbital-Angular-Momentum Coupled Bose-Einstein Condensate, Phys. Rev. Lett. **122**, 110402 (2019).

[10] Chunlei Qu, Lev P. Pitaevskii, and Sandro Stringari, Spin-orbit-coupling induced localization in the expansion of an interacting Bose-Einstein condensate, New J. Phys. **19**, 085006 (2017).

[11] A. J. Olson, D. B. Blasing, C. Qu, C.-H. Li, R. J. Niffenegger, C.-W. Zhang, and Y. P. Chen, Stueckelberg interferometry using periodically driven spin-orbit-coupled Bose-Einstein condensates, Phys. Rev. A **95**, 043623 (2017).

[12] C.-H. Li, C. Qu, R. J. Niffenegger, S.-J. Wang, M. He, D. B. Blasing, A. J. Olson, C. H. Greene, Y. Lyanda-Geller, Q. Zhou, C. Zhang, and Y. P. Chen, Spin current generation and relaxation in a quenched spin-orbit-coupled Bose-Einstein condensate, Nat. Commun. **10**, 375 (2019).

[13] C. Wang, C. Gao, C.-M. Jian, and H. Zhai, Spin-Orbit Coupled Spinor Bose-Einstein Condensates, Phys. Rev. Lett. **105**, 160403 (2010).

[14] T.-L. Ho and S. Zhang, Bose-Einstein Condensates with Spin-Orbit Interaction, Phys. Rev. Lett. **107**, 150403 (2011).

[15] C.-J. Wu, I. Mondragon-Shem, and X.-F. Zhou, Unconventional Bose-Einstein condensations from spin-orbit coupling, Chin. Phys. Lett. **28**, 097102 (2011).

[16] S. Sinha, R. Nath, and L. Santos, Trapped Two-Dimensional Condensates with Synthetic Spin-Orbit Coupling, Phys. Rev. Lett. **107**, 270401 (2011).

[17] Y. Zhang, L. Mao, and C. Zhang, Mean-Field Dynamics of Spin-Orbit Coupled Bose-Einstein Condensates, Phys. Rev. Lett. **108**, 035302 (2012).

[18] H. Hu, B. Ramachandhran, H. Pu, and X.-J. Liu, Spin-Orbit Coupled Weakly Interacting Bose-Einstein Condensates in Harmonic Traps, Phys. Rev. Lett. **108**, 010402 (2012).

[19] Y. Li, L. P. Pitaevskii, and S. Stringari, Quantum Tricriticality and Phase Transitions in Spin-Orbit Coupled Bose-Einstein Condensates, Phys. Rev. Lett. **108**, 225301 (2012).

[20] J.-R. Li, J. Lee, W. Huang, S. Burchesky, B. Shteynas, F. Ç. Top, A. O. Jamison, and W. Ketterle, A stripe phase with supersolid properties in spin-orbit-coupled Bose-Einstein condensates, Nature (London) **543**, 91 (2017).

[21] M. A. Khamehchi, Y. Zhang, C. Hamner, Th. Busch, and P. Engels, Measurement of collective excitations in a spin-orbit-coupled Bose-Einstein condensate, Phys. Rev. A **90**, 063624 (2014).

[22] S.-C. Ji, L. Zhang, X.-T. Xu, Z. Wu, Y. Deng, S. Chen, and J.-W. Pan, Softening of Roton and Phonon Modes in a Bose-Einstein Condensate with Spin-Orbit Coupling, Phys. Rev. Lett. **114**, 105301 (2015).

[23] V. Achilleos, D. J. Frantzeskakis, P. G. Kevrekidis, and D. E. Pelinovsky, Matter-Wave Bright Solitons in Spin-Orbit Coupled Bose-Einstein Condensates, Phys. Rev. Lett. **110**, 264101 (2013).

[24] Y. Xu, Y. Zhang, and B. Wu, Bright solitons in spin-orbit-coupled Bose-Einstein condensates, Phys. Rev. A **87**, 013614 (2013).

[25] H. Sakaguchi and B. A. Malomed, Flipping-shuttle oscillations of bright one- and two-dimensional solitons in spin-orbit-coupled Bose-Einstein condensates with Rabi mixing, Phys. Rev. A **96**, 043620 (2017).

[26] E. Chiquillo, Quasi-one-dimensional spin-orbit- and Rabi-coupled bright dipolar Bose-Einstein-condensate solitons, Phys. Rev. A **97**, 013614 (2018).

[27] O. Fialko, J. Brand, and U. Zülicke, Soliton magnetization dynamics in spin-orbit-coupled Bose-Einstein condensates, Phys. Rev. A **85**, 051605(R) (2012).

[28] L. Wen, Q. Sun, Y. Chen, D.-S. Wang, J. Hu, H. Chen, W.-M. Liu, G. Juzeliūnas, B. A. Malomed, and A.-C. Ji, Motion of solitons in one-dimensional spin-orbit-coupled Bose-Einstein condensates, Phys. Rev. A **94**, 061602(R) (2016).

[29] F. Kh. Abdullaev, M. Brtka, A. Gammal, and L. Tomio, Solitons and Josephson-type oscillations in Bose-Einstein condensates

with spin-orbit coupling and time-varying Raman frequency, Phys. Rev. A **97**, 053611 (2018).
[30] Q. Zhu, C. Zhang, and B. Wu, Exotic superfluidity in spin-orbit coupled Bose-Einstein condensates, Europhys. Lett. **100**, 50003 (2012).
[31] Y.-C. Zhang, Z.-W. Zhou, B. A. Malomed, and H. Pu, Stable Solitons in Three Dimensional Free Space without the Ground State: Self-Trapped Bose-Einstein Condensates with Spin-Orbit Coupling, Phys. Rev. Lett. **115**, 253902 (2015).
[32] Sh. Mardonov, E. Ya. Sherman, J. G. Muga, H.-W. Wang, Y. Ban, and X. Chen, Collapse of spin-orbit-coupled Bose-Einstein condensates, Phys. Rev. A **91**, 043604 (2015).
[33] L. Salasnich, W. B. Cardoso, and B. A. Malomed, Localized modes in quasi-two-dimensional Bose-Einstein condensates with spin-orbit and Rabi couplings, Phys. Rev. A **90**, 033629 (2014).
[34] H. Sakaguchi, E. Ya. Sherman, and B. A. Malomed, Vortex solitons in two-dimensional spin-orbit-coupled Bose-Einstein condensates: Effects of the Rashba-Dresselhaus coupling and Zeeman splitting, Phys. Rev. E **94**, 032202 (2016).
[35] Y. Xu, Y. Zhang, and C. Zhang, Bright solitons in a two-dimensional spin-orbit-coupled dipolar Bose-Einstein condensate, Phys. Rev. A **92**, 013633 (2015).
[36] X. Jiang, Z. Fan, Z. Chen, W. Pang, Y. Li, and B. A. Malomed, Two-dimensional solitons in dipolar Bose-Einstein condensates with spin-orbit coupling, Phys. Rev. A **93**, 023633 (2016).
[37] Y. Li, Y. Liu, Z. Fan, W. Pang, S. Fu, and B. A. Malomed, Two-dimensional dipolar gap solitons in free space with spin-orbit coupling, Phys. Rev. A **95**, 063613 (2017).
[38] Y. V. Kartashov and V. V. Konotop, Solitons in Bose-Einstein Condensates with Helicoidal Spin-Orbit Coupling, Phys. Rev. Lett. **118**, 190401 (2017).
[39] J. Radić, T. A. Sedrakyan, I. B. Spielman, and V. Galitski, Vortices in spin-orbit-coupled Bose-Einstein condensates, Phys. Rev. A **84**, 063604 (2011).
[40] X.-F. Zhou, J. Zhou, and C. Wu, Vortex structures of rotating spin-orbit-coupled Bose-Einstein condensates, Phys. Rev. A **84**, 063624 (2011).
[41] B. Ramachandhran, B. Opanchuk, X.-J. Liu, H. Pu, P. D. Drummond, and H. Hu, Half-quantum vortex state in a spin-orbit-coupled Bose-Einstein condensate, Phys. Rev. A **85**, 023606 (2012).
[42] C.-F. Liu, H. Fan, Y.-C. Zhang, D.-S. Wang, and W.-M. Liu, Circular-hyperbolic skyrmion in rotating pseudo-spin-1/2 Bose-Einstein condensates with spin-orbit coupling, Phys. Rev. A **86**, 053616 (2012).
[43] K. Kasamatsu, Dynamics of quantized vortices in Bose-Einstein condensates with laser-induced spin-orbit coupling, Phys. Rev. A **92**, 063608 (2015).
[44] L. A. Toikka, Vortex force in compressible spin-orbit-coupled Bose-Einstein condensates, Phys. Rev. A **96**, 033611 (2017).
[45] Y.-K. Liu and S.-J. Yang, Exact solitons and manifold mixing dynamics in the spin-orbit-coupled spinor condensates, Europhys. Lett. **108**, 30004 (2014).
[46] S. Gautam and S. K. Adhikari, Mobile vector soliton in a spin-orbit coupled spin-1 condensate, Laser Phys. Lett. **12**, 045501 (2015).
[47] S. Gautam and S. K. Adhikari, Vortex-bright solitons in a spin-orbit-coupled spin-1 condensate, Phys. Rev. A **95**, 013608 (2017).
[48] S. Gautam and S. K. Adhikari, Three-dimensional vortex-bright solitons in a spin-orbit-coupled spin-1 condensate, Phys. Rev. A **97**, 013629 (2018).
[49] Y.-E. Li and J.-K. Xue, Stationary and moving solitons in spin-orbit-coupled spin-1 Bose-Einstein condensates, Front. Phys. **13**, 130307 (2018).
[50] D. Ma and C. Jia, Soliton oscillation driven by spin-orbit coupling in spinor condensates, Phys. Rev. A **100**, 023629 (2019).
[51] S. K. Adhikari, Phase separation of vector solitons in spin-orbit-coupled spin-1 condensates, Phys. Rev. A **100**, 063618 (2019).
[52] S. Gautam and S. K. Adhikari, Vector solitons in a spin-orbit-coupled spin-2 Bose-Einstein condensate, Phys. Rev. A **91**, 063617 (2015).
[53] N.-S. Wan, Y. E. Li, and J.-K. Xue, Solitons in spin-orbit-coupled spin-2 spinor Bose-Einstein condensates, Phys. Rev. E **99**, 062220 (2019).
[54] Y. V. Kartashov, V. V. Konotop, and F. Kh. Abdullaev, Gap Solitons in a Spin-Orbit-Coupled Bose-Einstein Condensate, Phys. Rev. Lett. **111**, 060402 (2013).
[55] V. E. Lobanov, Y. V. Kartashov, and V. V. Konotop, Fundamental, Multipole, and Half-Vortex Gap Solitons in Spin-Orbit Coupled Bose-Einstein Condensates, Phys. Rev. Lett. **112**, 180403 (2014).
[56] Y. Zhang, Y. Xu, and Th. Busch, Gap solitons in spin-orbit-coupled Bose-Einstein condensates in optical lattices, Phys. Rev. A **91**, 043629 (2015).
[57] H. Sakaguchi and B. A. Malomed, One- and two-dimensional gap solitons in spin-orbit-coupled systems with Zeeman splitting, Phys. Rev. A **97**, 013607 (2018).
[58] H. Li, S.-L. Xu, M. R. Belić, and J.-X. Cheng, Three-dimensional solitons in Bose-Einstein condensates with spin-orbit coupling and Bessel optical lattices, Phys. Rev. A **98**, 033827 (2018).
[59] Sh. Mardonov, V. V. Konotop, B. A. Malomed, M. Modugno, and E. Ya. Sherman, Spin-orbit-coupled soliton in a random potential, Phys. Rev. A **98**, 023604 (2018).
[60] Y. V. Kartashov and D. A. Zezyulin, Stable Multiring and Rotating Solitons in Two-Dimensional Spin-Orbit-Coupled Bose-Einstein Condensates with a Radially Periodic Potential, Phys. Rev. Lett. **122**, 123201 (2019).
[61] V. Achilleos, D. J. Frantzeskakis, and P. G. Kevrekidis, Beating dark-dark solitons and Zitterbewegung in spin-orbit-coupled Bose-Einstein condensates, Phys. Rev. A **89**, 033636 (2014).
[62] S. Cao, C.-J. Shan, D.-W. Zhang, X. Qin, and J. Xu, Dynamical generation of dark solitons in spin-orbit-coupled Bose-Einstein condensates, J. Opt. Soc. Am. B **32**, 201 (2015).
[63] X.-W. Luo, K. Sun, and C. Zhang, Spin-Tensor-Momentum-Coupled Bose-Einstein Condensates, Phys. Rev. Lett. **119**, 193001 (2017).
[64] H. Hu, J. Hou, F. Zhang, and C. Zhang, Topological Triply Degenerate Points Induced by Spin-Tensor-Momentum Couplings, Phys. Rev. Lett. **120**, 240401 (2018).
[65] M.-Xue Guan, C. Lian, S.-Qi Hu, H. Liu, S.-Jie Zhang, J. Zhang, and S. Meng, Cooperative evolution of intraband and

interband excitations for high-harmonic generation in strained MoS_2, Phys. Rev. B **99**, 184306 (2019).

[66] Y.-J. Lin, R. L. Compton, A. R. Perry, W. D. Phillips, J. V. Porto, and I. B. Spielman, Bose-Einstein Condensate in a Uniform Light-Induced Vector Potential, Phys. Rev. Lett. **102**, 130401 (2009).

[67] D. Campbell, R. Price, A. Putra, A. Valdés-Curiel, D. Trypogeorgos, and I. B. Spielman, Magnetic phases of spin-1 spin-orbit-coupled Bose gases, Nat. Commun. **7**, 10897 (2016).

[68] Y. Zhang, M. E. Mossman, Th. Busch, P. Engels, and C. Zhang, Properties of spin-orbit-coupled Bose-Einstein condensates, Front. Phys. **11**, 118103 (2016).